Spatial and Wavenumber Resolution of Doppler Reflectometry

Evgeniy Gusakov, Alexander Surkov

Spatial and Wavenumber Resolution of Doppler Reflectometry

E Z Gusakov and A V Surkov

Ioffe Institute, Politekhnicheskaya 26, 194021 St. Petersburg, Russia

E-mail: Evgeniy.Gusakov@mail.ioffe.ru, a.surkov@mail.ioffe.ru

Abstract. Doppler reflectometry spatial and wavenumber resolution is analyzed within the framework of the linear Born approximation in slab plasma model. Explicit expression for its signal backscattering spectrum is obtained in terms of wavenumber and frequency spectra of turbulence which is assumed to be radially statistically inhomogeneous. Scattering efficiency for both back and forward scattering (in radial direction) is introduced and shown to be inverse proportional to the square of radial wavenumber of the probing wave at the fluctuation location thus making the spatial resolution of diagnostics sensitive to density profile. It is shown that in case of forward scattering additional localization can be provided by the antenna diagram. It is demonstrated that in case of backscattering the spatial resolution can be better if the turbulence spectrum at high radial wavenumbers is suppressed. The improvement of Doppler reflectometry data localization by probing beam focusing onto the cut-off is proposed and described. The possibility of Doppler reflectometry data interpretation based on the obtained expressions is shown.

Submitted to: *Plasma Phys. Control. Fusion*

PACS numbers: 52.70.Gw, 52.35.Hr, 52.35.Ra

1. Introduction

Plasma rotation velocity measurements are of great importance for understanding transition to improved confinement in tokamaks and physics of transport barriers. Extensively used nowadays for such investigations is Doppler reflectometry [1, 2, 3]. This technique provides measuring fluctuations propagation poloidal velocity which is often shown to be dominated by $\vec{E} \times \vec{B}$ velocity of plasma [3]. In using this method a probing microwave beam is launched into the plasma with finite tilt angle with respect to density gradient. A back-scattered signal with frequency differing from the probing one is registered by a nearby standing or the same antenna. The information on plasma poloidal rotation is obtained in this technique from the frequency shift of the backscattering spectrum which is supposed to originate from the Doppler effect due to the fluctuation rotation. Spatial distribution of the scattering phenomena, which is usually assumed to occur in the cut-off vicinity, is the key issue for the diagnostic applications.

Some numerical simulations undertaken (see [3] and references there, [4]) and analytical results [5] demonstrate the possibility of the measurements localization by the cut-off but the problem of Doppler reflectometry locality remains still open and lacks comprehensive analytical treatment. This stems from the fact that to be sure that main contribution to the registered signal is made by the cut-off vicinity one should compare it with integral contributions of distant from the cut-off regions which can be substantial depending on density profile.

This paper attempts to clarify this problem. Here we present a theoretical investigation of the Doppler reflectometry signal dependence on the turbulence distribution with respect to the cut-off. We consider slab two-dimensional model (see figure 1). This simplification allows us to perform straightforward analytical treatment and obtain explicit reliable expressions for the scattered signal which can be easily used for estimation of diagnostics locality and experimental data interpretation without complicated and time consuming numerical calculation using full-wave codes, etc. The model considered can be readily applied to large in comparison with probing beam width, vertically elongated (ITER-like) plasma. The limitations of this approximation are discussed below.

The paper is organized as follows. In section 2 the consideration is carried on in the geometrical optics approximation for arbitrary plasma density profile. This approximation fails to hold in the cut-off region. So in this region the analysis is made assuming the density profile to be linear and using exact expressions for the probing and scattered wave electric field given by Airy functions (section 3). Some numerical examples are given in section 4. Brief discussion of the model considered and results obtained is provided in section 5. Finally, a conclusion follows in section 6.

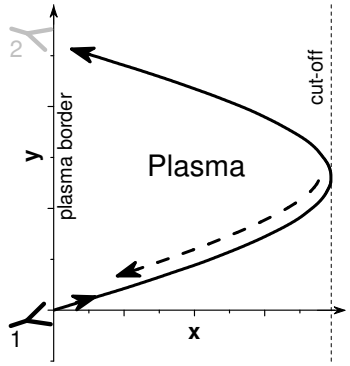

Figure 1. Diagnostics scheme. 1—emitting and receiving antenna, 2—additional receiving antenna (to be discussed in section 5).

2. Reflectometry signal in WKB–approximation

In this section the reflectometry signal is obtained in geometrical optics (or WKB) approximation. The plasma is assumed to be nonuniform in x (radial) direction and uniform in y (poloidal) direction. External magnetic field is supposed to be along z axis. O-mode Doppler reflectometry is considered but the final results can be easily adapted to X-mode reflectometry applying corresponding expression for wave radial wavenumber dependence on the radial coordinate.

A received signal is obtained using reciprocity theorem [6] and is assumed to be created by single scattering (linear) mechanism. The frameworks of this approximation and experimental means to check its applicability are discussed in section 5. The scattering signal averaging is made taking into account radial statistical inhomogeneity of the turbulence. Then a scattering efficiency is introduced and analyzed.

2.1. Scattering signal

We consider normalized antenna electric field in the following form

$$\vec{E}_a(\vec{r}) = \vec{e}_z \int\limits_{-\infty}^{+\infty} \frac{\mathrm{d}k_y}{2\pi} W(x, k_y) f(k_y) \mathrm{e}^{\mathrm{i}k_y y}$$

where factor $f(k_y)$ takes into account the antenna pattern describing antenna radiation in vacuum

$$f(k_y) = \sqrt{\frac{c}{8\pi}} \int\limits_{-\infty}^{+\infty} dy E_0(x=0, y) \mathrm{e}^{-\mathrm{i}k_y y}$$

The vacuum antenna field E_0 differs from E_a by the absence of the reflected wave contribution.

Here and further we suppose the probing wave to oscillate at frequency ω and omit the corresponding term in equations. Radial electric field distribution is described by

the function $W(x, k_y)$ which is determined by

$$W'' + k_x^2(x, k_y)W = 0 \tag{1}$$

where the square of ordinary wave wavevector radial projection is given by $k_x^2(x, k_y) = k^2(x) - k_y^2 = [\omega^2 - \omega_{pe}^2(x)]/c^2 - k_y^2$. Thus ordinary wave electric field in WKB-approximation has the following form [7]:

$$W(x, k_y) = 4\sqrt{\frac{2\pi\omega}{c^2 k_x(x, k_y)}} \exp\left[\mathrm{i}\int_0^{x_c(k_y)} k_x(x', k_y)\,\mathrm{d}x' - \frac{\mathrm{i}\pi}{4}\right] \times \cos\left[\frac{\pi}{4} - \int_x^{x_c(k_y)} k_x(x', k_y)\,\mathrm{d}x'\right]$$

where the turning point $x_c(k_y)$ is determined by the equation

$$k_x\left[x_c(k_y), k_y\right] = 0$$

and $x = 0$ corresponds to the plasma border.

Using reciprocity theorem [6, 7], an amplitude of the received scattering signal at frequency $\omega_s = \omega + \Omega$, where Ω denotes the frequency of the fluctuation caused the scattering, can be written as

$$A_s(\omega_s) = \frac{\mathrm{i}e^2}{4m_e\omega}\sqrt{P_i}\int_{-\infty}^{+\infty} \delta n_\Omega(\vec{r}) E_a^2(\vec{r})\,\mathrm{d}\vec{r}$$

Here P_i is the probing wave power. Following the model considered the fluctuations are assumed to be long enough along the magnetic field direction z, so their dependence on z can be neglected. Introducing the density perturbation Fourier harmonic

$$\delta n(\varkappa, q, \Omega) = \int_{-\infty}^{+\infty} \delta n(x, y, \Omega)\mathrm{e}^{-\mathrm{i}\varkappa x - \mathrm{i}qy}\mathrm{d}x\mathrm{d}y$$

we obtain

$$A_s(\omega_s) = \frac{\mathrm{i}\pi e^2}{2m_e\omega}\sqrt{P_i}\int_{-\infty}^{+\infty} \frac{\mathrm{d}k_y\,\mathrm{d}\varkappa\,\mathrm{d}q}{(2\pi)^3}\,\delta n(\varkappa, q, \Omega) f(k_y) f(-k_y - q) C(\varkappa, q, k_y) \tag{2}$$

The efficiency of scattering off the fluctuation with radial wavenumber $\varkappa$ and poloidal wavenumber q has the following form [7]

$$\begin{aligned} C(\varkappa, q, k_y) &= \int_{-\infty}^{+\infty} W(x, k_y) W(x, -k_y - q)\mathrm{e}^{\mathrm{i}\varkappa x}\mathrm{d}x \\ &= \int_{-\infty}^{+\infty} \frac{\mathrm{d}x}{\sqrt{k_x(x, k_y)k_x(x, -k_y - q)}} \sum_{m,n=\pm 1} \mathrm{e}^{\mathrm{i}\Psi_{mn} - \mathrm{i}(m+n)\pi/4} \\ \Psi_{mn} &= \varkappa x + m\phi(x, k_y) + n\phi(x, -k_y - q) + \phi(0, k_y) + \phi(0, -k_y - q) \\ \phi(x, k_y) &= \int_x^{x_c(k_y)} k_x(x', k_y)\,\mathrm{d}x' \end{aligned}$$

The scattering efficiency $C(\varkappa, q, k_y)$ is an integral of the oscillating function. Main contribution to this integral is made by stationary phase points. Following [7] to estimate

this integral let us calculate this contribution. Equalizing the derivative of the phase to zero one obtains the Bragg condition

$$\varkappa - mk_x(x_*, k_y) - nk_x(x_*, -k_y - q) = 0 \tag{3}$$

In nonuniform plasma this determines the scattering point x_*

$$k^2(x_*) = \left[\frac{\varkappa}{2} + \frac{q(2k_y + q)}{2\varkappa}\right]^2 + k_y^2 \tag{4}$$

The figures m, n are related to different cases of scattering.

$$m = \operatorname{sgn}\frac{\varkappa^2 + q(2k_y + q)}{\varkappa}, \quad n = \operatorname{sgn}\frac{\varkappa^2 - q(2k_y + q)}{\varkappa} \tag{5}$$

As it will be shown below case $m = n$ corresponds to the backscattering (BS) and $m = -n$ accords to the forward scattering (FS). The sign of m is related to the scattering before ($m = -1$) and after ($m = 1$) the cut-off in respect of the probing wave propagation. Equations (5) express the fact that one fluctuation can scatter the wave only once. The situation, for example, when the wave with fixed k_y is forward scattered off the fluctuation far from the cut-off and the same wave can be scattered backward off the same fluctuation near the cut-off is impossible. This circumstance will allow us below to separate the contributions of forward and backward scattering processes.

The final expression for the scattering efficiency in WKB approximation takes the form

$$C(\varkappa, q, k_y) = 2\sqrt{\frac{\pi\ell_*^3}{|\varkappa|}} \exp\left[\mathrm{i}\Psi_{mn}(x_*) + \frac{\mathrm{i}\pi}{4}\operatorname{sgn}(mn\varkappa)\right]$$

where $\ell_* = \left[\partial k^2(x)/\partial x|_{x=x_*}\right]^{-1/3}$ is local Airy scale. Introducing local density variation scale $L_* = \left[\mathrm{d}\ln n_e(x)/\mathrm{d}x|_{x=x_*}\right]^{-1}$ we obtain for ordinary probing wave $\ell_* = \left[c^2 L_*/\omega_{pe}^2(x_*)\right]^{1/3}$.

On substituting the obtained expression for the scattering efficiency into (2) we obtain the received signal

$$A_s = 4\pi^{3/2}\frac{e^2}{m_e c^2}\sqrt{P_i}\int_{-\infty}^{+\infty}\frac{\mathrm{d}k_y\,\mathrm{d}\varkappa\,\mathrm{d}q}{(2\pi)^3}\,\delta n(\varkappa, q, \Omega) f(k_y) f(-k_y - q)\frac{\ell_*^{3/2}}{\sqrt{\varkappa - \mathrm{i}o}}\,\mathrm{e}^{\mathrm{i}\Psi(x_*, k_y)} \tag{6}$$

where $o > 0$ determines how the integration path goes around the singularity. Here $\Psi(x_*, k_y) = \Psi_{mn}$, where m, n is determined by (5).

2.2. Scattering signal analysis: integration over k_y

We calculate the integral over k_y in (6) using saddle point method. It is especially efficient if the cut-off is far enough from the antenna and does not coincide with the focal point of the antenna beam, so that the ray tracing consideration is applicable. In this case the saddle point k_y^* is determined by the stationary point of the phase $\Phi = \Psi(x_*, k_y) + \arg f(k_y) + \arg f(-k_y - q)$ and the $|f(k_y)f(-k_y - q)|$ dependence on

k_y is negligible. Corresponding criterion to distinguish this and opposite case will be formulated below.

In this "ray tracing" case the stationary phase condition

$$\left.\frac{\mathrm{d}\Phi\left[x_*(k_y),k_y\right]}{\mathrm{d}k_y}\right|_{k_y=k_y^*}=0 \tag{7}$$

can be easily interpreted. At first we consider the meaning of $\mathrm{d}\Psi/\mathrm{d}k_y$ term. Recollecting that

$$k_x^2(x,k_y)=k^2(x)-k_y^2 \tag{8}$$

and

$$\frac{\partial\phi(x,k_y)}{\partial k_y}=-k_y\int_x^{x_c(k_y)}\frac{\mathrm{d}x'}{k_x(x',k_y)}$$

one obtains

$$\begin{aligned}\frac{\partial\Psi}{\partial k_y}=&-mk_y\int_{x_*}^{x_c(k_y)}\frac{\mathrm{d}x}{k_x(x,k_y)}-n(k_y+q)\int_{x_*}^{x_c(-k_y-q)}\frac{\mathrm{d}x}{k_x(x,-k_y-q)}\\&-k_y\int_0^{x_c(k_y)}\frac{\mathrm{d}x}{k_x(x,k_y)}-(k_y+q)\int_0^{x_c(-k_y-q)}\frac{\mathrm{d}x}{k_x(x,-k_y-q)}\end{aligned} \tag{9}$$

Taking into account that (8) yields the following relation between the projections of group velocities $\vec{v}_g=\partial\omega/\partial\vec{k}$ of incident and scattered waves:

$$\frac{v_{gy}^{(i)}}{v_{gx}^{(i)}}=\frac{k_y}{k_x(x,k_y)},\qquad\frac{v_{gy}^{(s)}}{v_{gx}^{(s)}}=\frac{-k_y-q}{k_x(x,-k_y-q)}$$

we obtain

$$\frac{\partial\Psi}{\partial k_y}=-m\int_{x_*}^{x_c(k_y)}\frac{v_{gy}^{(i)}}{v_{gx}^{(i)}}\,\mathrm{d}x-\int_0^{x_c(k_y)}\frac{v_{gy}^{(i)}}{v_{gx}^{(i)}}\,\mathrm{d}x+n\int_{x_*}^{x_c(-k_y-q)}\frac{v_{gy}^{(s)}}{v_{gx}^{(s)}}\,\mathrm{d}x+\int_0^{x_c(-k_y-q)}\frac{v_{gy}^{(s)}}{v_{gx}^{(s)}}\,\mathrm{d}x \tag{10}$$

Now one can see that $\Delta y=-\partial\Psi/\partial k_y$ corresponds to shift of the ray trajectory along y direction when it returns to the antenna. In less general case it was mentioned in [8]. For instance, if $m=-n=1$ then (10) takes the form

$$\frac{\partial\Psi}{\partial k_y}=-\int_0^{x_c(k_y)}\frac{v_{gy}^{(i)}}{v_{gx}^{(i)}}\,\mathrm{d}x-\int_{x_c(k_y)}^{x_*}\frac{v_{gy}^{(i)}}{-v_{gx}^{(i)}}\,\mathrm{d}x-\int_{x_*}^{0}\frac{v_{gy}^{(s)}}{v_{gx}^{(s)}}\,\mathrm{d}x$$

and $(-\partial\Psi/\partial k_y)$ is the shift of the ray trajectory in case of forward scattering after the reflection off the turning point. Here the meaning of the figures m,n (5) announced above becomes clear.

Accounting for the influence of the wavefront curvature at the antenna given by $\arg f(k_y)\neq 0$ we consider gaussian antenna pattern

$$f(k_y)=\sqrt{2\sqrt{\pi}\rho}\mathrm{e}^{-(\rho^2-\mathrm{i}c\mathcal{R}/\omega)(k_y-\mathcal{K})^2/2} \tag{11}$$

In case of

$$c\mathcal{R}/\omega\gg\rho^2 \tag{12}$$

parameter $\mathcal{R}$ has a meaning of a wavefront curvature radius at the antenna. In (11) $\mathcal{K}$ corresponds to the antenna tilt ($\mathcal{K} = \omega/c \sin\vartheta$, where ϑ denotes tilt angle in respect of the density gradient). This allows us to obtain condition (7) in the form

$$\frac{\mathrm{d}\Phi}{\mathrm{d}k_y} = -\Delta y + \frac{c\mathcal{R}}{\omega}(2k_y + q) = 0 \tag{13}$$

Taking into account that the ray with poloidal wavevector component k_y is radiated from the position $y(k_y) = -k_y\mathcal{R}c/\omega$ of the curved wavefront at the antenna which is assumed to be situated in the axes origin, it is easy to show that (13) determines a ray trajectory which returns to the proper point of the antenna wavefront after the scattering off the fluctuation with wavevector $(\varkappa, q)$.

To get explicit expression for the stationary point position k_y^* we use paraxial approximation. Supposition of small divergence of the antenna beam $|k_y - \mathcal{K}| \ll \omega/c$ which holds usually in the experiments on Doppler reflectometry [3] allows us to write

$$k_x(x, k_y) \approx k_x(x, \mathcal{K}) - \frac{k_y^2 - \mathcal{K}^2}{2k_x(x, \mathcal{K})}$$

and neglect the dependence on k_y in denominators in (9). This allows us to obtain

$$\frac{\partial\Psi}{\partial k_y} = -\frac{ck_y}{\omega}\left[(m+n)\Lambda(x_*) + 2\Lambda_0\right] - \frac{cq}{\omega}\left[n\Lambda(x_*) + \Lambda_0\right]$$

$$\Lambda(x) = \frac{\omega}{c}\int_x^{x_c(\mathcal{K})} \frac{\mathrm{d}x'}{k_x(x', \mathcal{K})}, \quad \Lambda_0 \equiv \Lambda(0)$$

Using (7) we get the stationary phase point position

$$k_y^* = \begin{cases} -q/2, & \text{m=n} \\ -q/2\left[1 + n\Lambda(x_*)/(\Lambda_0 - \mathcal{R})\right], & \text{m=-n} \end{cases} \tag{14}$$

for the BS and FS respectively.

In the opposite case when ray trajectories consideration is not valid k_y^* is determined by the antenna pattern amplitude

$$\left.\frac{\mathrm{d}|f(k_y)f(-k_y - q)|}{\mathrm{d}k_y}\right|_{k_y = k_y^*} = 0$$

yielding $k_y^* = -q/2$ for an arbitrary antenna pattern.

The assumption of gaussian antenna pattern (11) allows us to evaluate the saddle point position in general case

$$k_y^* = -\frac{q}{2}\frac{\Lambda_0 - \mathcal{R} + n\Lambda(x_*) - \mathrm{i}\mathcal{P}}{\Lambda_0 - \mathcal{R} + (m+n)/2 \cdot \Lambda(x_*) - \mathrm{i}\mathcal{P}}$$

where $\mathcal{P} = \omega\rho^2/c$ and formulate the criterion in question. The ray tracing consideration is valid if $\rho^2 \ll c|\Lambda_0 - \mathcal{R}|/\omega$ and thus the focal point is not too close to the cut-off. If the focal point is situated in the cut-off $\rho^2 \gg c|\Lambda_0 - \mathcal{R}|/\omega$ we come to the expression $k_y^* = -q/2$.

Using stationary k_y^* calculated above and performing the integration we obtain the scattering signal in the following form

$$A_s = 2\pi \frac{e^2}{m_e c^2} \sqrt{P_i} \int_{-\infty}^{+\infty} \frac{\mathrm{d}\varkappa\, \mathrm{d}q}{(2\pi)^2}\, \delta n(\varkappa, q, \Omega) \times f\left[k_y^*(\varkappa, q)\right] f\left[-k_y^*(\varkappa, q) - q\right] \ell_*^{3/2} \frac{\Delta(\varkappa, q)}{\sqrt{\varkappa - \mathrm{i}o}} \mathrm{e}^{\mathrm{i}\Psi(x_*, k_y^*)}$$

where

$$\Delta(\varkappa, q) = \left\{ \rho^2 - \mathrm{i}\left[\frac{c\mathcal{R}}{\omega} + \frac{1}{2} \frac{d^2\Psi\left[x_*(k_y), k_y\right]}{\mathrm{d}k_y^2} \right] \right\}^{-1/2}$$

2.3. Scattering signal averaging

We consider the turbulence to be slightly inhomogeneous along x direction so that the density fluctuation correlation function takes the form

$$\langle \delta n(x) \delta n(x') \rangle = \delta n^2 \left(\frac{x + x'}{2} \right) \int_{-\infty}^{+\infty} \frac{\mathrm{d}\varkappa}{2\pi} \left| \tilde{n}\left(\varkappa, q, \Omega, \frac{x + x'}{2} \right) \right|^2 \mathrm{e}^{\mathrm{i}\varkappa(x - x')} \tag{15}$$

This representation is applicable when the turbulence correlation length along x axis ℓ_{cx} is much smaller than the turbulence inhomogeneity scale. It allows us to take into account the dependence of turbulence on the radial coordinate and still describe it using wavenumber spectrum $|\tilde{n}\left[\varkappa, q, \Omega, (x + x')/2\right]|^2$. Supposing the turbulence to be stationary and homogeneous in y-direction and using (15) we can represent correlation function of spectral density in the form

$$\langle \delta n(\varkappa, q, \Omega) \delta n^*(\varkappa', q', \Omega') \rangle = \int_{-\infty}^{+\infty} \mathrm{d}x\, \delta n^2(x) \left| \tilde{n}\left(\frac{\varkappa + \varkappa'}{2}, q, \Omega, x \right) \right|^2 \times \mathrm{e}^{\mathrm{i}x(\varkappa - \varkappa')} (2\pi)^2 \delta(q - q') \delta(\Omega - \Omega')$$

where the integration is performed over all plasma volume. It allows spectral power density of the received signal to be represented in the following form

$$p(\omega_s) = \langle A_s \bar{A}_s \rangle = P_i \int_{-\infty}^{+\infty} \mathrm{d}x\, \delta n^2(x) S(x) \tag{16}$$

where $\bar{A}_s$ is complex conjugate to A_s.

The scattering efficiency $S(x)$ introduced here takes the form

$$S(x) = 4\pi^2 \left(\frac{e^2}{m_e c^2} \right)^2 \int_{-\infty}^{+\infty} \frac{\mathrm{d}\varkappa\, \mathrm{d}\varkappa'\, \mathrm{d}q}{(2\pi)^3} \left| n\left(\frac{\varkappa + \varkappa'}{2}, q, \Omega, x \right) \right|^2 \times f\left[k_y^*(\varkappa, q)\right] f\left[-k_y^*(\varkappa, q) - q\right] \overline{f\left[k_y^*(\varkappa', q)\right]}\, \overline{f\left[-k_y^*(\varkappa', q) - q\right]} \times (\ell_* \ell_*')^{3/2} \frac{\Delta(\varkappa, q) \Delta(\varkappa', q)}{\sqrt{\varkappa \varkappa'}}\, \mathrm{e}^{\mathrm{i}x(\varkappa - \varkappa') + \mathrm{i}\Psi[\varkappa, q] - \mathrm{i}\Psi[\varkappa', q]}$$

and determines actually the Doppler reflectometry locality and wavenumber resolution. Performing the integration over $\varkappa - \varkappa'$ using stationary phase method we obtain

$$S(x) \approx (2\pi)^{3/2} \left(\frac{e^2}{m_e c^2} \right)^2 \int_{-\infty}^{+\infty} \frac{\mathrm{d}\varkappa\, \mathrm{d}q}{(2\pi)^2} \left| \tilde{n}(\varkappa, q, \Omega, x) \right|^2 \left| f\left[k_y^*(\varkappa, q)\right] \right|^2 \left| f\left[-k_y^*(\varkappa, q) - q\right] \right|^2$$

$$\times \ell_*^3 \frac{|\Delta(\varkappa,q)|^2}{|\varkappa|\sqrt{|x'_{*\varkappa}|}} \exp\left\{\frac{\mathrm{i}\left[x-x_*(\varkappa,q)\right]^2}{2x'_{*\varkappa}(\varkappa,q)} - \frac{\mathrm{i}\pi}{4}\mathrm{sgn}x'_{*\varkappa}(\varkappa,q)\right\} \tag{17}$$

where $x'_{*\varkappa}(\varkappa,q) \equiv \partial x_*(\varkappa,q)/\partial\varkappa$ and the scattering point position $x_*(\varkappa,q)$ is given by (3).

One can see that due to the oscillating term $\exp\left\{\mathrm{i}\left[x-x_*(\varkappa,q)\right]^2/\left(2x'_{*\varkappa}(\varkappa,q)\right)\right\}$ the main input to the integral (17) is provided by the stationary point $x = x_*$. It corresponds to the contribution of the fluctuations producing scattering just in the point x.

Here we suppose the fluctuation spectral density $|\tilde{n}(\varkappa,q,\Omega,x)|^2$ to vary with $\varkappa$ slow enough in comparison with the oscillating term. In general case four terms arise from condition $x_*(\varkappa,q) = x$ which is equivalent to

$$k\left[x_*(\varkappa^*,q)\right] = k(x) \tag{18}$$

where $k(x_*)$ is determined by (4) and $k_y = k_y^*$ is substituted according to section 2.2. Solving (18) and taking interest in "stationary" $\varkappa^*$ we obtain

$$\varkappa^*_{m,n} = mk_x(x,k_y^*) + n\sqrt{k_x^2(x,k_y^*) - q(2k_y^*+q)} \tag{19}$$

Figures m and n have the same meaning as above but here and further they are independent parameters and specify corresponding solutions of (18).

To distinguish contributions of different scattering types we represent the scattering efficiency in the following form

$$S(x) = \pi\left(\frac{e^2}{m_e c^2}\right)^2 \int_{-\infty}^{+\infty} \frac{\mathrm{d}q}{2\pi}\left[S_{BS}(x,q) + S_{FS}(x,q)\right] \tag{20}$$

and discuss the properties of back and forward scattering efficiency separately.

2.4. BS efficiency

To obtain the two terms corresponding to the backscattering which occur before or after reflection of the probing wave we substitute $m = n$ and $k_y^* = -q/2$ to (19) according to (14). This yields

$$\varkappa^*_{m,m} = 2mk_x\left(x,-\frac{q}{2}\right), \quad m = \pm 1$$

and

$$|x'_{*\varkappa}| = \ell_*^3 k_x\left(x,-\frac{q}{2}\right)$$

$$\left|\Delta(\varkappa^*_{m,m},q)\right|^2 = \left\{\rho^4 + \frac{c^2}{\omega^2}\left[\Lambda_0 - \mathcal{R} + m\Lambda(x)\right]^2\right\}^{-1/2}$$

It allows us to obtain BS contribution in question

$$S_{BS}(x,q) = \frac{|f(-q/2)|^4}{k_x^2(x,\mathcal{K})} \sum_{m=\pm 1} \frac{\left|\tilde{n}\left[2mk_x(x,\mathcal{K}),q,\Omega,x\right]\right|^2}{\sqrt{\rho^4 + c^2\left[\Lambda_0 - \mathcal{R} + m\Lambda(x)\right]^2/\omega^2}} \tag{21}$$

It can be seen that the contributions of the BS before (m=n=-1) and after (m=n=1) the cut-off have different amplitudes due to the diffraction effect dependence on length of the ray trajectory from emitting to receiving antenna.

We consider main features of the BS efficiency (21) obtained. The first factor determining the localization of BS signal which appears to be typical for the fluctuation reflectometry [9] is $k^{-2}(x)$. Just recently [9] the same factor was revealed in analysis of correlation matrix of phase perturbations of fluctuation reflectometry signal in nonlinear regime. It is maximal in the vicinity of the cut-off where in the WKB approximation it has singularity. This singularity saturation will be treated in details in section 3. This maximum explained by the growth of the probing and scattered wave electric filed in the cut-off provides the technique with spatial localization, however, the decay of $k^{-2}(x)$ when leaving cut-off is not fast enough to guarantee suppression of the signal coming from wide edge region. Moreover, for quite a few density profiles (e.g. linear and bent down ones) the integral of $k^{-2}(x)$ over x does not converge due to far from the cut-off regions. So plasma periphery contribution can be essential in these cases. The illustration of this effect is given in section 4.

Additional possibility to increase selectively the BS signal coming from the cut-off can be provided by focusing the beam of probing and receiving antennae to the cut-off region. This corresponds to $\mathcal{R} = \Lambda_0$ in (21). In this case the focusing causes additional growth at the cut-off of probing and scattered wave amplitudes leading to the scattered signal enhancement similar to that predicted for the cut-off or upper hybrid resonance [10].

The two mentioned effects increasing the probing wave electric field substantially in the cut-off should enhance the locality of the Doppler reflectometry diagnostics making it less sensitive to the backscattering in the edge plasma.

The backscattering locality can be also better for some fluctuation radial wavenumber spectra. One can see from (21) that if the short-scale fluctuations are suppressed enough in the spectrum the backscattering contribution will be essential in the cut-off vicinity only.

2.5. FS efficiency

To calculate the FS terms we use ray-tracing consideration. Substituting $m = -n$ to (19) we obtain

$$\varkappa^*_{m,-m} = \frac{q^2\Lambda(x)}{2k_x(x,k_y^*)(\Lambda_0 - \mathcal{R})}$$

It is noteworthy that both $\varkappa^*_{m,-m}$ have the same sign and differ only slightly due to different values of k_y^* only.

Finally we obtain

$$|x'_{*\varkappa}| = \frac{2c(\Lambda_0 - \mathcal{R})}{\omega q^2} k_x(x,k_y^*)k_x(x,-k_y^*-q)\left|\frac{\omega\Lambda(x)}{2cL_*k_x(x,k_y^*)} - 1\right|^{-1}$$

$$\left|\Delta(\varkappa^*_{m,-m},q)\right|^2 = \left(\rho^4 + \frac{c^2(\Lambda_0-\mathcal{R})^2}{\omega^2}\right)^{-1/2}\left|1 - \frac{2cL_*k_x(x,k_y^*)}{\omega\Lambda(x)}\right|^{-1}$$

Thus the sum of two similar forward scattering terms corresponding to the scattering before and after the turning point takes a form

$$S_{FS}(x,q) = \frac{2}{\sqrt{\rho^4 + c^2(\Lambda_0 - \mathcal{R})^2/\omega^2}} \left| f\left\{ -\frac{q}{2}\left[1 + \frac{\Lambda(x)}{\Lambda_0 - \mathcal{R}}\right]\right\}\right|^2 \times \left| f\left\{ -\frac{q}{2}\left[1 - \frac{\Lambda(x)}{\Lambda_0 - \mathcal{R}}\right]\right\}\right|^2 \frac{1}{k_x^2(x,\mathcal{K})} \left|\tilde{n}\left[\frac{q^2\Lambda(x)}{2k(x)(\Lambda_0 - \mathcal{R})}, q, \Omega, x\right]\right|^2 \quad (22)$$

The main reason for the mentioned similarity is equal trajectory length in this case. It is worth noting that if $\mathcal{R} < \Lambda_0$ the forward scattering efficiency S_{FS} is contributed to by the fluctuations with positive radial wavenumbers only.

Substituting gaussian antenna power diagram (11) into (22) we obtain expression for the factor describing antenna pattern influence in the following form

$$\left| f\left[-\frac{q}{2}\left(1 + \frac{\Lambda(x)}{\Lambda_0 - \mathcal{R}}\right)\right]\right|^2 \left| f\left[-\frac{q}{2}\left(1 - \frac{\Lambda(x)}{\Lambda_0 - \mathcal{R}}\right)\right]\right|^2 = 4\pi\rho^2 \exp\left\{ -\frac{\rho^2}{2}\left[(q + 2\mathcal{K})^2 + \left[\frac{q\Lambda(x)}{\Lambda_0 - \mathcal{R}}\right]^2\right]\right\} \quad (23)$$

Additional contribution to the forward scattering efficiency can be provided by singularities of the term $|\Delta(\varkappa, q)|^2 / |\varkappa|$ in (17). As it is shown in Appendix A it is small at substantial distance from the cut-off where the condition

$$\frac{ck(x)}{\omega} > \rho\sqrt{\frac{\omega}{c(\Lambda_0 - \mathcal{R})}}\left(\frac{12}{\alpha}\right)^{1/2} \quad (24)$$

holds. Here $\alpha = |L_*^2/n_e(x_c) \cdot \mathrm{d}^2 n_e(x)/\mathrm{d}x^2||_{x=x_c}$ characterizes the nonlinearity of the density profile. If the cut-off is not close to the focal point, so that $\rho\sqrt{\omega/[c(\Lambda_0 - \mathcal{R})]} \ll 1$ the expression (22) for the FS contribution appears to be valid where nonlinear corrections to $k^2(x)$ are still small. Closer to the cut-off where inequality (24) is not satisfied the contribution of the branching point to the integral in (17) is important. It is calculated below taking into account that the density profile in this region can be treated as linear. The corresponding contribution doubles the result for the FS signal.

Similar to (21) FS efficiency (22) is also proportional to $k^{-2}(x)$. However unlike (21) the cut-off contribution is not enhanced there by probing wave focusing. In this case the focusing merely compensates the refraction of probing beam leading to FS signal amplitude growth in all plasma volume. It can be seen from (22) that FS signal is contributed to by long-scale fluctuations, which disable the third possible localizing factor discussed for BS — turbulence spectrum.

Nevertheless, according to (22), (23) the extra localization of the forward scattering can be due to the fact that FS signal coming from plasma volume is received in Doppler reflectometry is received by the antenna pattern periphery. Supposing gaussian antenna beam to be wide enough, the integration over q yields the following estimation of the forward scattering efficiency

$$S_{FS}(x) = \pi\left(\frac{e^2}{m_e c^2}\right)^2 \int_{-\infty}^{+\infty} \frac{\mathrm{d}q}{2\pi} S_{FS}(x,q)$$

$$\approx \left(\frac{e^2}{m_e c^2}\right)^2 \frac{2\,(2\pi)^{3/2}\,\omega\rho}{c(\Lambda_0-\mathcal{R})k_x^2(x)} \exp\left\{-2\left[\frac{\rho\mathcal{K}\Lambda(x)}{\Lambda_0-\mathcal{R}}\right]^2\right\}$$
$$\times \left|\tilde{n}\left[\frac{2\mathcal{K}^2\Lambda(x)}{k(x)(\Lambda_0-\mathcal{R})}, -2\mathcal{K}, \Omega, x\right]\right|^2$$

Thus the factor describing the antenna pattern effect decreases rapidly in moving off the cut-off under condition the beam is wide enough or sufficiently tilted. If the antenna beam focusing to the cut-off is provided this localizing factor can be even more essential.

3. Scattering signal in the cut-off vicinity

The explicit expressions for the scattering efficiency (21), (22) were obtained in the previous section using WKB and ray tracing consideration. These expressions possesses singularities when validity conditions for WKB approach

$$k^{-2}(x)\frac{\mathrm{d}k(x)}{\mathrm{d}x} \ll 1 \tag{25}$$

and ray tracing consideration

$$\rho^2 \ll \left|\frac{c(\Lambda_0-\mathcal{R})}{\omega}\right|$$

are violated in the cut-off vicinity.

To analyze the scattering efficiency in this region a more rigorous approach is needed. To do that we recollect that in the cut-off vicinity the density profile can be represented as linear $k^2(x) = (x_c - x)/\ell^3$ where $\ell = (c^2L/\omega^2)^{1/3}$ is the Airy scale and $L = [\mathrm{d}\ln n_e(x)/\mathrm{d}x|_{x=x_c}]^{-1}$ is local density variation scale in the cut-off position. In this case the criterion (25) takes the form $k(x)\ell \gg 1$.

Then in the cut-off vicinity the radial distribution of the ordinary wave electric field has the following form [7]:

$$W(x,k_y) = \sqrt{\frac{8\omega\ell}{c^2}} \exp\left[\mathrm{i}\int_0^{x_c(k_y)} k_x(x',k_y)\,\mathrm{d}x' - \frac{\mathrm{i}\pi}{4}\right]$$
$$\times \int_{-\infty}^{+\infty} \exp\left[\frac{\mathrm{i}p^3}{3} + (\xi + k_y^2\ell^2)p\right]\,\mathrm{d}p$$

where $\xi = (x - x_c)/\ell$.

According to the reciprocity theorem [6] the scattering signal has the following structure

$$A_s = \frac{\mathrm{i}e^2}{4m_e\omega}\sqrt{P_i}\int \mathrm{d}x \int_{-\infty}^{+\infty} \frac{\mathrm{d}k_y\,\mathrm{d}\varkappa\,\mathrm{d}q}{(2\pi)^3}\,\delta n(\varkappa,q,\Omega)\mathrm{e}^{\mathrm{i}\varkappa(x-x_c)}$$
$$\times f(k_y)f(-k_y-q)W(x,k_y)W(x,-k_y-q) \tag{26}$$

As we have already done assuming moderate spatial inhomogeneity of the turbulence (15) and calculating the integral over k_y in (26) by stationary phase method

we transform the registered signal spectral power density to the form (16). For the scattering efficiency we get

$$S(x) \approx \frac{4\pi\ell^3}{\sqrt{\rho^4 + c^2(\Lambda_0 - \mathcal{R})^2/\omega^2}} \left(\frac{e^2}{m_e c^2}\right)^2 \times \int_{-\infty}^{+\infty} \frac{\mathrm{d}\varkappa\,\mathrm{d}q}{(2\pi)^2} \left|\tilde{n}(\varkappa, q, \Omega, x)\right|^2 \left|f\left(-\frac{q}{2}\right)\right|^4 R(x, \varkappa, q) \tag{27}$$

$$R(x, \varkappa, q) = \int_{-\infty}^{+\infty} \frac{\mathrm{d}\tau}{\sqrt{(\beta - \theta)^2 - (\tau + \mathrm{i}\epsilon)^2}} \exp\left\{\frac{\mathrm{i}\tau^3}{6} + \frac{\mathrm{i}\tau}{2}\left(\beta^2 - K^2\right)\right\} \tag{28}$$

where the following notation is used

$$\beta = \varkappa\ell, \quad \theta = \frac{L\ell c q^2}{\omega} \frac{\Lambda_0 - \mathcal{R}}{(\Lambda_0 - \mathcal{R})^2 + \mathcal{P}^2}, \quad \epsilon = \frac{\mathcal{P}\theta}{\Lambda_0 - \mathcal{R}}, \quad K = 2\ell k_x\left(x, -\frac{q}{2}\right)$$

The expression for $R(x, \varkappa, q)$ can be simplified in two cases. In the first one $K \gg \theta$ and the position of the turbulence x is far from the cut-off. Omitting oscillating terms hardly having an effect in integrating over β we can distinguish two characteristic ranges of fluctuation radial wavenumbers. The fist one corresponds to $|\beta| \ll K$. Considering such fluctuations, which are responsible for the forward scattering we can approximate

$$R \approx R^{(1)}(x, \varkappa, q) = 2\pi \mathrm{J}_0\left[\frac{1}{2}K^2\left|\beta - \theta\right|\right] \mathrm{e}^{-\epsilon K^2} \tag{29}$$

The second group of wavenumbers corresponds to $|\beta| \sim K$. These fluctuations provide the backscattering in this region. Corresponding expression of the scattering efficiency has the following form

$$R \approx R^{(2)}(x, \varkappa, q) = \frac{2^{4/3}\pi}{|\beta|} \mathrm{Ai}\left[\frac{\beta^2 - K^2}{2^{2/3}}\right] \tag{30}$$

Assuming the spectral density $\left|\tilde{n}(\varkappa, q, \Omega, x)\right|^2$ to vary with $\varkappa$ slow enough and neglecting this variation when performing the integration over $\varkappa$ which is correct for distances from the cut-off $x_c - x > \ell_{cx}$ where ℓ_{cx} is radial correlation length of the turbulence, we represent the scattering efficiency in form (20) and get the forward scattering contribution

$$S_{FS}(x, q) = 4\left[\rho^4 + \frac{c^2(\Lambda_0 - \mathcal{R})^2}{\omega^2}\right]^{-1/2} \frac{\left|f\left(-q/2\right)\right|^4}{k_x^2\left(x, -q/2\right)} \left|\tilde{n}\left(\frac{Lcq^2}{\omega}\frac{\Lambda_0 - \mathcal{R}}{(\Lambda_0 - \mathcal{R})^2 + \mathcal{P}^2}, q, \Omega, x\right)\right|^2 \times \exp\left\{-\frac{2(\rho q L)^2}{(\Lambda_0 - \mathcal{R})^2 + \mathcal{P}^2}\left[\frac{c k_x\left(x, -q/2\right)}{\omega}\right]^2\right\} \tag{31}$$

and backscattering one

$$S_{BS}(x, q) = \left[\rho^4 + \frac{c^2(\Lambda_0 - \mathcal{R})^2}{\omega^2}\right]^{-1/2} \frac{\left|f\left(-q/2\right)\right|^4}{k_x^2\left(x, -q/2\right)} \sum_{\pm} \left|\tilde{n}\left[\pm 2k_x\left(x, -q/2\right), q, \Omega, x\right]\right|^2 \tag{32}$$

This BS efficiency expression matches when leaving the cut-off corresponding WKB formula (21) obtained for the arbitrary density profile whereas the FS contribution (31) exceeds corresponding WKB result (22) by the factor of 2. Taking into account the

discussion of the previous section we can write approximate formula describing the transition from (22) to (31) which happens when nonlinear correction to the density profile decreases.

$$S_{FS}(x,q) \sim 4\frac{1+\gamma^2}{1+2\gamma^2}k^{-2}(x,\mathcal{K})\left|f\left(-\frac{q}{2}\right)\right|^4 \exp\left\{-\frac{1}{2}\frac{\left[\rho q\Lambda(x)\right]^2}{(\Lambda_0-\mathcal{R})^2+\mathcal{P}^2}\right\}$$
$$\times\left[\rho^4+\frac{c^2(\Lambda_0-\mathcal{R})^2}{\omega^2}\right]^{-1/2}\left|\tilde{n}\left[\frac{q^2\Lambda(x)}{2k(x)}\frac{\Lambda_0-\mathcal{R}}{(\Lambda_0-\mathcal{R})^2+\mathcal{P}^2},q,\Omega,x\right]\right|^2 \qquad (33)$$

where as above $\mathcal{P}=\omega\rho^2/c$ and $\gamma = ck(x)/(\omega\rho)\sqrt{\alpha c(\Lambda_0-\mathcal{R})/(12\omega)}$.

Expressions (31), (32) and (33) for the scattering efficiency describe the transition from the ray tracing consideration to the case of probing beam focusing to the cut-off both for the gaussian and arbitrary antenna pattern. In the last case we determine parameters ρ, $\mathcal{R}$ as:

$$\rho^2 = -\Re\frac{f''(\mathcal{K})}{f^2(\mathcal{K})}, \qquad \mathcal{R} = \Im\frac{\omega f''(\mathcal{K})}{cf^2(\mathcal{K})}$$

In case when ray tracing approximation fails to hold, which can be provided by large antenna beam width $\rho^2 > c\Lambda_0/\omega$ or by the focusing to the cut-off $\mathcal{R}\sim\Lambda_0$, the FS contribution takes the following form

$$S_{FS}(x,q) \approx 4\left[\rho k(x)\right]^{-2}\left|f\left(-\frac{q}{2}\right)\right|^4 \exp\left\{-\frac{1}{2}\left(\frac{cq}{\omega}\right)^2\left[\frac{\Lambda(x)}{\rho}\right]^2\right\}\left|\tilde{n}\left[0,q,\Omega,x\right]\right|^2$$

Equation (21) for BS contribution holds true in general situation ($\mathcal{P}\lesseqgtr|\Lambda_0-\mathcal{R}|$) for arbitrary antenna pattern providing the redefining of ρ and $\mathcal{R}$ mentioned above is made.

The second important case to be considered is when the turbulence is situated near the cut-off $K\lesssim 1$ where WKB scattering efficiency has singularity. Main contribution to the scattering in this location can be shown to be due to fluctuations with $|\beta|<K$. It is given by

$$R(x,\varkappa,q) \sim 2\pi \mathrm{J}_0\left[\frac{1}{2}\left(K^2-\beta^2\right)|\beta-\theta|\right]\mathrm{e}^{-\epsilon\left(K^2-\beta^2\right)/2}-\pi$$
$$-2\int_0^\infty\frac{\mathrm{d}\tau}{\tau}\sin\left[\frac{\tau^3}{6}+\frac{\tau}{2}\left(\beta^2-K^2\right)\right]$$

This expression reveals a scattering efficiency maximum to be situated near $K\approx 2.3$ which corresponds to $k(x)\sim 1.15/\ell$ or $x_c-x\sim 1.3\ell$. A numerical calculation of function $R(x,\varkappa,q)$ with following integration over $\varkappa$ confirms this result. Figure 2 represents numerical results (black dots) in case of short-scale fluctuations $\ell_{cx}\ll\ell$. Here for the sake of clarity the fluctuations spectral density is supposed to be constant in (27) during the integration over $\varkappa$.

Additionally this computation shows WKB formulae (21), (22) for scattering efficiency to be valid up to the maximum providing k_x in denominators is replaced by

$$k_x \leftrightarrow k_x - 0.5/\ell \qquad (34)$$

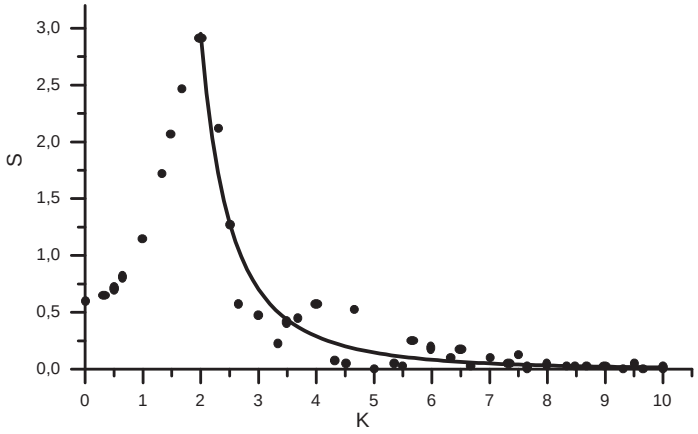

Figure 2. Scattering efficiency calculated numerically (•) and analytically (solid line) vs. $K = 2k_x(x, -q/2)\ell$.

(solid line in figure 2). Oscillations near this solid line correspond to the oscillating term omitted in (29) which can be shown not to contribute essentially to the resulting scattered signal magnitude due to averaging provided by slow spatial variation of the fluctuation amplitude. Fast decay of S for $k_x < 0.5/\ell$ is caused by the probing wave field decrease in the evanescent region.

In integration over $\varkappa$ in expressions (17), (29), (30) we neglected the influence of the fluctuation spectral density $|\tilde{n}(\varkappa, q, \Omega, x)|^2$. Now we consider the case $\ell_{cx} \gg \ell$ when this approximation is not valid. In this case of long-scale turbulence the backscattering contribution is small in comparison with forward scattering one and can be neglected

$$S(x) \approx \pi \left(\frac{e^2}{m_e c^2}\right)^2 \int_{-\infty}^{+\infty} \frac{\mathrm{d}q}{2\pi} S_{FS}(x, q)$$

According to (27), (29) the scattering efficiency takes the form

$$S_{FS}(x, q) \approx \frac{2c}{\omega\ell} \left| f\left(-\frac{q}{2}\right)\right|^4 \mathrm{e}^{-\epsilon K^2} \int_{-\infty}^{+\infty} \mathrm{d}\beta \left|\tilde{n}\left(\frac{\beta}{\ell}, q, \Omega, x\right)\right|^2 \mathrm{J}_0\left[\frac{1}{2}K^2\,|\beta - \theta|\right] \tag{35}$$

The characteristic scale of the spectral density variation with $\beta = \varkappa\ell$ is ℓ/ℓ_{cx}. The corresponding scale for the term $\mathrm{J}_0\left[1/2K^2\,|\beta - \theta|\right]$ is $\delta\beta \sim K^{-2}$. In evaluating last integral in (35) two cases can be distinguished. Far from the cut-off at $x_c - x \gg \ell_{cx}$ the integral converges due to the Bessel function at $\beta \sim \delta\beta \ll \ell/\ell_{cx}$. It gives k_x^{-2}-behavior for the scattering efficiency which was obtained above (31).

In the opposite case $x_c - x \lesssim \ell_{cx}$ the integral in (35) converges due to the turbulence spectrum at $\beta \sim \ell/\ell_{cx}$ leading to the saturation of the singularity k_x^{-2}. This saturation is described analytically in the case of gaussian fluctuation spectral density

$$|\tilde{n}\,(\varkappa, q, \Omega)|^2 = 2\sqrt{\pi}\ell_{cx}\,|\tilde{n}\,(q, \Omega)|^2\,\mathrm{e}^{-\ell_{cx}^2\varkappa^2}$$

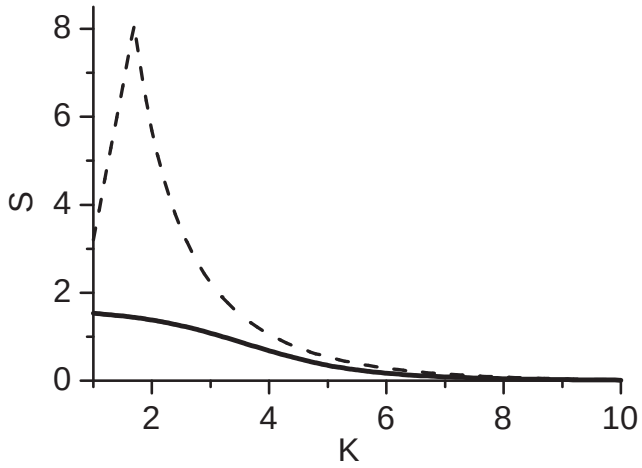

Figure 3. Approximation of scattering efficiency for $\ell_{cx} \gg \ell$ (solid line $\ell_{cx} = 2$ cm, $\ell = 0.5$ cm) and $\ell_{cx} \ll \ell$ (dashed line) vs. $K = 2k_x(x, -q/2)\ell$.

which allows the integral over β in (35) to be calculated exactly

$$\int_{-\infty}^{+\infty} \mathrm{d}\beta \left|\tilde{n}\left(\frac{\beta}{\ell}, q, \Omega, x\right)\right|^2 \mathrm{J}_0\left[\frac{1}{2}K^2\,|\beta - \theta|\right] \approx 2\pi\ell\,|\tilde{n}\,(q, \Omega, x)|^2 \exp\left(-\frac{K^4\ell^2}{32\ell_{cx}^2}\right) \mathrm{I}_0\left(\frac{K^4\ell^2}{32\ell_{cx}^2}\right)$$

where I_0 is modified Bessel function.

The difference in scattering efficiency behavior for small-scale ($\ell_{cx} \ll \ell$) and long-scale turbulence ($\ell_{cx} \gg \ell$) is illustrated by figure 3. In our case the transition to the plateau occurs in the point $K^2 \sim 4\ell_{cx}/\ell$ which gives

$$x_c - x \sim \ell_{cx}$$

To summarize, in the case $\ell_{cx} \ll \ell$ in approaching the cut-off the scattering efficiency grows, has maximum in the point $x_c - x \sim 1.3\ell$ and diminishes when $x_c - x < \ell$ due to probing wave field decrease in the evanescent region. When $\ell_{cx} \gg \ell$ the scattering efficiency has a plateau in the region $x_c - x \lesssim \ell_{cx}$.

4. Estimation of experiment locality

On performing the correction (34) the WKB-formulae (21), (22) can be used up to the cut-off vicinity. We consider simple model illustrating main properties of the scattering efficiency obtained. Geometrical parameters taken correspond to Tore Supra experiments [1], where cut-off being situated in the antenna near-field zone ($\omega/c \sim 12.6$ cm^{-1}, $\rho \sim 14$ cm, distance to the cut-off $L \sim 20$ cm). Let us assume bent down plasma density profile (figure 4(a)) similar to observed in Tore Supra [11] and step-like plasma poloidal velocity distribution (figure 4(b)). For the sake of simplicity

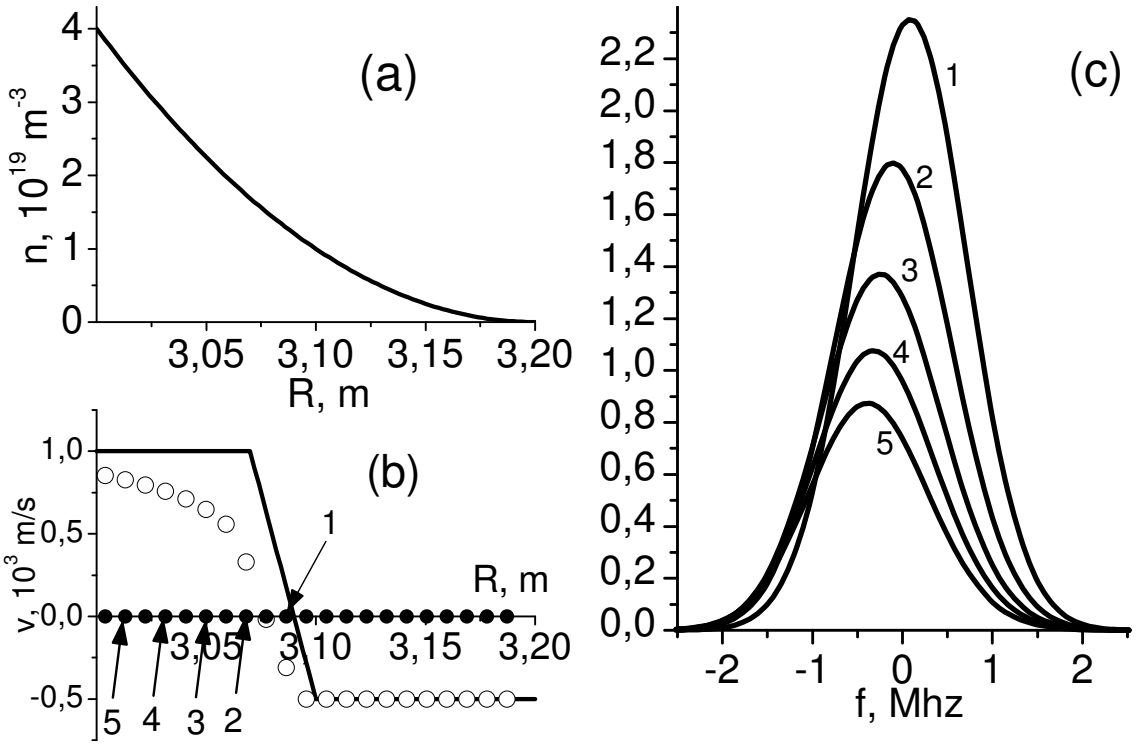

Figure 4. Signal spectrum evolution. (a) Assumed density profile. Horizontal axe is equivalent to the major radius. Probing is performed from right-hand side. (b) Poloidal velocity profile (solid line), cut-off positions (•) and velocity estimated using frequency spectrum shift (○). (c) Signal spectrum corresponding to the cut-off positions marked on (b).

we assume the turbulence level to be uniform (which looks like real situation when relative turbulence amplitude $\delta n/n$ increases in approaching plasma periphery) and the wavenumber spectra to be gaussian.

The probing is performed at different frequencies and therefore with different cut-off positions. We assume probing antenna to provide constant tilt angle $\vartheta = 11.5°$ and will calculate corresponding probing wave poloidal wavenumber $\mathcal{K} = \omega/c \sin\vartheta$ for each frequency.

We take into account scattered signal frequency shift due to the Doppler effect in the final expression for the scattering efficiency therefore assuming arising additional dependence on radial coordinate $|\tilde{n}\,[\ldots,\ldots,\Omega - qv(x)]|^2$ to be slow enough. We perform the integration over q in (32), (33) assuming the antenna pattern (11) to be wide enough to determine the behavior of integrand and calculate spectral power density (16) of the registered signal. Spectra obtained are represented in figure 4(c).

Turbulence correlation length was taken small $\ell_c \sim 0.1$ cm, Airy length being $\ell \sim 0.5$ cm. So the turbulence spectrum did not improve enough the locality and one can see that contribution of long area with $v = -0.5 \cdot 10^5$ cm/s (see figure 4(b)) is essential for spectra 1–3 (figure 4(c)). It can be seen that these spectra Doppler shifts do not accord the velocity in corresponding cut-off positions (see figure 4(d)).

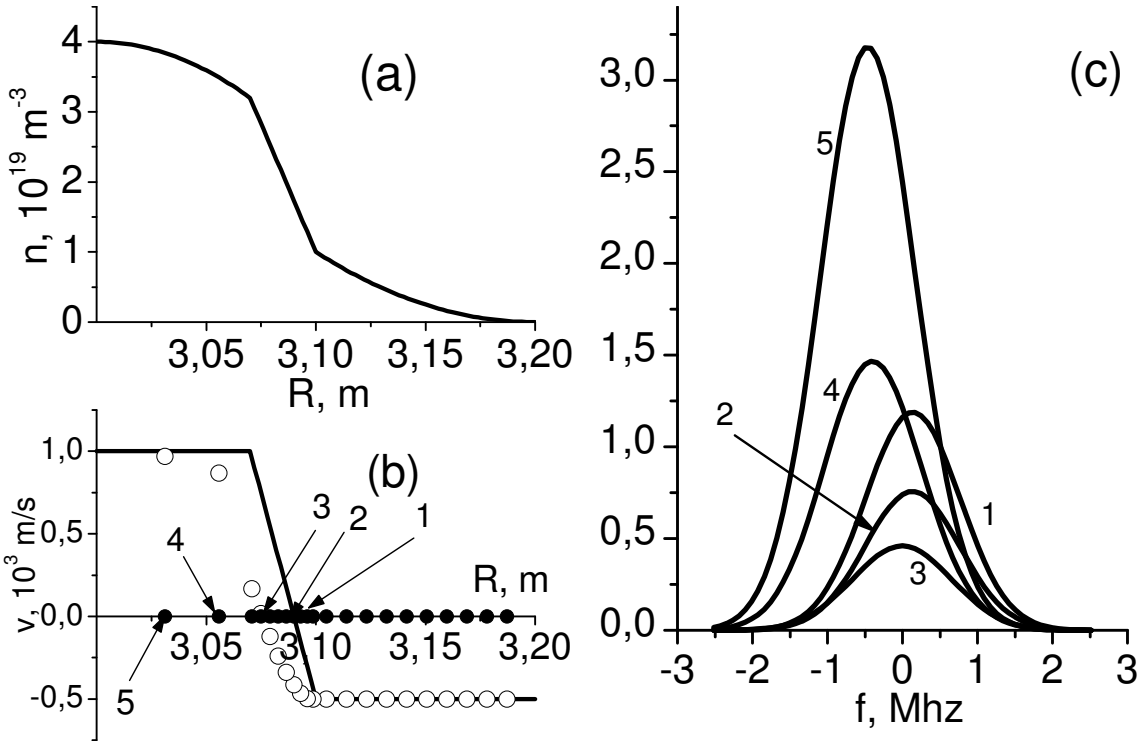

Figure 5. Signal spectrum evolution. (a) Assumed density profile. Horizontal axe is equivalent to the major radius. Probing is performed from right-hand side. (b) Poloidal velocity profile (solid line), cut-off positions (•) and velocity estimated using frequency spectrum shift (○). (c) Signal spectrum corresponding to the cut-off positions marked on (b).

It is necessary to move cut-off deep inside the plasma (spectra 4, 5) to provide the dominance of the region behind the velocity step point. Thus poor locality of Doppler reflectometry associated with bend down density profile in this situation can obscure the velocity distribution.

Diagnostics localization dependence on plasma density profile is also demonstrated by the next example simulating a transport barrier. We consider plasma density profile (figure 5(a)) bent down in plasma periphery and bent up in the core. The poloidal velocity profile has high gradient in the "barrier" region (figure 5(b)). One can see that up to cut-off position 3 frequency spectrum shift (see spectra 1–3, figure 5(c)) accords to negative poloidal rotation velocity corresponding to the plasma periphery. But on crossing the twist point by the cut-off position the signal grows and the frequency shift changes to that corresponding to the local value of the velocity in the cut-off region (cf. spectra 4, 5, figure 5(c) and figure 5(d)). This illustrates the better locality of the method when used on bent up density profile.

To illustrate antenna focusing influence we consider the density profile of DIII-D tokamak plasma with internal transport barrier (figure 6(a)) [12]. Here we take into account the distance between antenna and the plasma, which was assumed to be equal 1 m, and suppose that the probing is performed with narrow antenna beam

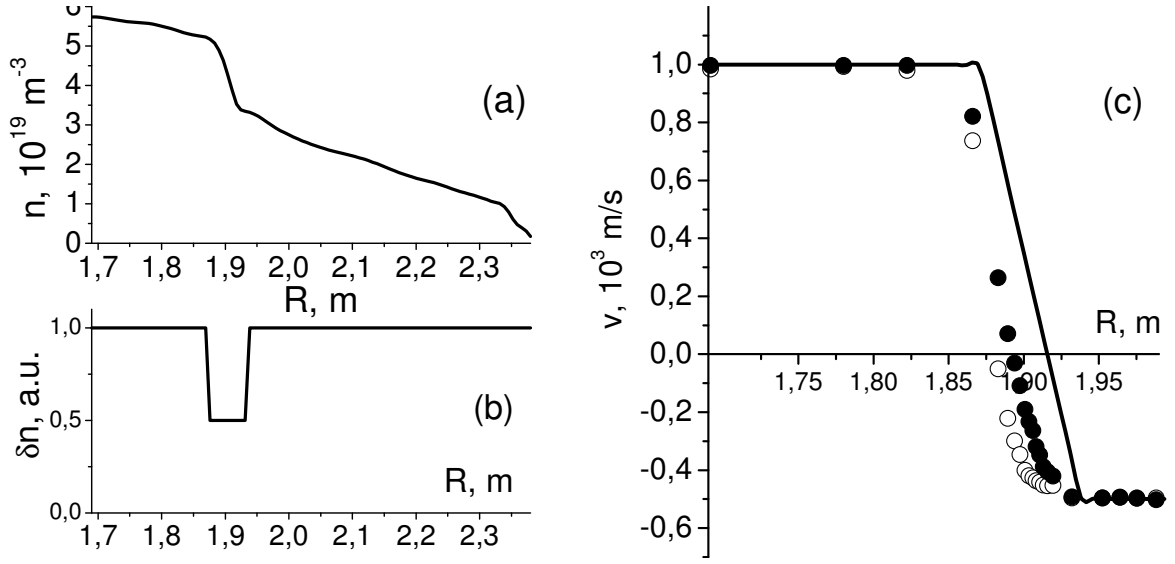

Figure 6. Antenna focusing influence. (a) DIII-D density profile [12]. (b) Turbulence amplitude assumed. (c) Poloidal velocity profile (solid line), and velocity estimated using Doppler reflectometry signal frequency spectrum shift: •—using antenna focusing, ∘—without focusing.

($\rho \sim 1$ cm) to provide condition (12) to be satisfied. Besides that we take into account the turbulence suppression in the barrier region (see figure 6(b)). Despite the fact that density profile in the barrier region is favorable for the diagnostics, antenna focusing makes the spectrum shift more adequate to the behavior of plasma velocity in the cut-off.

5. Discussion

First of all we discuss the frameworks of approximations used. In this paper we consider Doppler reflectometry in slab plasma geometry. As it was mentioned in section 1 this model is reliable for large vertically elongated plasma. The effects of cylindricalness become important when the probing beam width in the cut-off vicinity is comparable with the cut-off surface curvature radius which takes place in small toroidal devices or in case of probing of plasma central regions. These cases of essentially cylindrical plasma geometry were considered numerically in [13] and analytically (for specific plasma density profiles) in [14]. In these papers rather obvious conclusion was obtained that plasma poloidal curvature enhances the diagnostics sensitivity to the fluctuations with high poloidal wavenumbers. Another cylindrical geometry effect was investigated numerically in [15] where strong influence of the plasma cylindricalness on the diagnostics locality was demonstrated.

Essential can be the plasma poloidal curvature influence on the focused antenna beam. In the present paper it was neglected, which is correct, when the focus radial shift due to refraction associated with the plasma curvature is less than radial fluctuation

correlation length ℓ_{cx}. This criterion can be represented in form

$$2\Lambda_0 \frac{x_c}{r_0} < \ell_{cx}$$

Here Λ_0 is the ray trajectory length from the antenna to cut-off, which was defined above, x_c is the distance between the antenna and the cut-off and r_0 is the plasma radius in poloidal plane. Roughly this criterion can be approximated as $x_c^2/r_0 \lesssim \ell_{cx}$. When it fails to hold to provide the focusing to the cut-off the probing wavefront curvature radius should be calculated taking into account plasma poloidal curvature. All the mentioned effects will be taken into account in separate paper of the authors.

Additionally it should be noted that 2D plasma geometry effects like cylindricalness are not a priory significant in reflectometry (see e.g. [9, 16, 17], where it was demonstrated both analytically [9] and numerically [16, 17] that 2D theory predictions for radial correlation reflectometry are similar to conclusions of simple 1D model).

The second essential assumption made in the paper is associated with linear character of the scattering signal formation. According to [18] this approximation is correct when following criterion is satisfied

$$\frac{\delta n^2}{n_c^2} \frac{\omega^2 x_c \ell_{cx}}{c^2} \ln \frac{x_c}{\ell_{cx}} \ll 1 \tag{36}$$

Here δn is r.m.s amplitude of the turbulence and n_c denotes the density in the cut-off. It can be seen that (36) can be violated in case of high fluctuation amplitude or long trajectory length. In this case probing wave multi-scattering should be taken into account. This situation can be treated analytically by the procedure using in [18] and it will be done in the paper by the authors which is now under preparation for submission.

For diagnostics results interpretation it is important to distinguish linear and nonlinear situation. To do that experimentally one can use additional acquisition antenna (antenna 2 in figure 1) which receives the wave reflected from the cut-off. If the specular component persists in the frequency spectrum measured by this additional antenna the distortions of the probing wave in propagation are weak and we deal with linear situation of single-scattering. In the opposite case when the line at probing frequency is lost in the broadened reflection spectrum these distortions due to propagation in turbulent plasma lead to extinction of the specular component, which indicates transition to nonlinear small-angle multi-scattering regime. This way of experimental confirmation seems to be reliable but needs additional access to plasma. If it is impossible some information can be obtained from the form of Doppler reflectometry spectrum received by antenna 1 in figure 1. If the frequency spectrum width is consistent with estimation made based on the antenna pattern width ($\delta\omega \sim 2\sqrt{2}v/\rho$) one can conclude that the signal most likely resulted from single-scattering.

The scattering efficiency introduced and analytically obtained (21), (22) in the paper reveals main similarities and differences of conventional reflectometry and Doppler technique. In the both methods scattering signal is proportional to reversed square of probing wavenumber [9]. That provides the diagnostics with spatial localization, which can be rather poor in case of unfavorable density profile.

The back-scattering signal component formation is similar for tilted probing, which is performed in Doppler technique and normal probing which is specific for conventional method. In particular, in both cases the probing wave focusing to the cut-off, according to (21), underlines the cut-off region contribution and should improve the diagnostics localization. It is worth mentioning that utilization of non-slab probing wave fronts have been already discussed in [3, 19, 20], however in these papers the front curvature was chosen close to the cut off surface curvature in order to improve the Doppler reflectometry wave number resolution [3, 20], or to reduce the 2D interference effects in the signals reflected from different parts of corrugated cut off surface [19]. Finally it should be noted that 2D-focusing onto the cut-off surface, which can be easily realized in experiment, can provide even better localization than 1D-focusing only possible within 2D model considered in the present paper.

Essential are the peculiarities of FS efficiency (22). Both for Doppler and conventional reflectometry the cut-off contribution to the FS component is received by the most favorable part of the antenna diagram $k_y = -q/2$. However the suppression of the signal coming from the plasma volume in the case of conventional reflectometry takes place only for fluctuations satisfying condition $q\rho \gg 1$, at which the cut off contribution is suppressed as well. For longer poloidal scales $q^{-1} \geq \rho$ the suppression is not efficient and additional localization is not possible. On contrary for Doppler reflectometry due to the tilted probing the FS component of the signal, coming from the plasma volume is suppressed providing the following condition is fulfilled

$$\frac{\rho \mathcal{K} \Lambda_0}{\Lambda_0 - \mathcal{R}} \gg 1$$

It can be easily achieved by large enough antenna tilt angle or beam width, or by the focusing to the cut-off, thus making the FS contribution extremely localized to the cut-off.

Finally we discuss the wavenumber resolution of the Doppler reflectometry. The scattering efficiency obtained (21), (21) demonstrates that diagnostics possess practically no radial wavenumber resolution due to the fact that scattering signal is an integral over radial wavenumbers and small $\varkappa$ are pronounced with weight function $1/\varkappa$. Poloidal wavenumber resolution can be easily estimated and is determined by antenna pattern width. For BS contribution it can be represented as

$$\delta q \sim \frac{\sqrt{2}}{\rho}$$

FS poloidal wavenumber resolution can be $\sqrt{2}$ times worse.

6. Conclusion

In the present paper the Doppler reflectometry spatial and wavenumber resolution is analyzed in the framework of the linear Born approximation in slab plasma model. The results obtained provide realistic description of Doppler reflectometry experiment in large elongated plasma at low level of density perturbation.

Explicit expression for the backscattering spectrum is obtained in terms of wavenumber and frequency spectra of turbulence assumed to be statistically inhomogeneous in radial direction. The treatment is performed for arbitrary density profile and antenna pattern taking into account diffraction effects. In agreement with [3] it is demonstrated that the signal consists of contributions of back and forward scattering in radial direction, which take place both before and after the reflection of the probing wave in the turning point. Similar to the traditional fluctuation reflectometry [9] the scattering efficiency for both back and forward scattering is shown to be inverse proportional to the square of radial wavenumber of the probing wave at the fluctuation location thus making the spatial resolution of diagnostics sensitive to the density profile. It is shown that additional localization is provided in case of forward scattering in the radial direction by the antenna diagram and in case of backscattering by the fact that the turbulence spectrum is suppressed at high radial wavenumbers. The improvement of the diagnostics locality by probing beam focusing onto the cut-off surface is proposed described as well.

It is demonstrated that analytical expressions obtained can be easily used for fast interpretation of Doppler reflectometry data in particular for estimation of this diagnostics locality. They can as well serve for benchmarking and testing of full wave numerical codes developed for interpretation of conventional fluctuation reflectometry data [13, 14, 15, 16, 17, 21], should the authors consider the application of these codes to the field of Doppler reflectometry.

The magnetic surfaces curvature, if important, can be accounted for within the same theoretical approach applied to cylindrical plasma geometry. The nonlinear effects in Doppler reflectometry spectra formation becoming significant in large devices and at high density perturbation level can be described within WKB approximation in the way similar to one used in [18].

Acknowledgments

We would like to thank Dr. V.V. Bulanin (St.-Petersburg State Polytechnical University) who drew our attention to the importance of the probing wave front curvature for the diagnostic performance.

This paper was subsidized by RFBR grants 02-02-17589, 04-02-16534, State support of leading scientific schools program (project no. 2159.2003.2), INTAS grant 01-2056 and NWO-RFBR grant 047.009.009. One of the authors (A.V.S.) is grateful to the Dynasty foundation for supporting his research.

Appendix A.

Here we estimate additional contribution to the forward scattering efficiency (22), which can be provided by singularities of the term $|\Delta(\varkappa, q)|^2 / |\varkappa|$ in (17). This term possesses

four branching points which in ray tracing case are determined by equations

$$\varkappa_{1-4} = \pm\frac{q^2}{\Lambda_0 - \mathcal{R}}\left[\frac{cL_*\Lambda_*}{\omega k\left[x_*\left(\varkappa_{1-4}\right)\right]}\right]^{1/2}\left(1 \pm \frac{\mathrm{i}\omega\rho^2}{2c(\Lambda_0 - \mathcal{R})}\right)$$

where L_*, Λ_* are taken in the scattering point $x_*\left(\varkappa_{1-4}\right)$ corresponding to $\varkappa_{1-4}$. The branching point contribution is especially large in the cut-off vicinity where $k^2(x) = \omega^2/c^2(x_c - x)/L_*$ and

$$\Lambda(x) = \frac{2cL_*}{\omega}k(x)$$

The real part of right branching points $\varkappa_b \equiv \Re\varkappa_{1,4}$ in this case coincides with the stationary phase point $\varkappa^* \equiv \varkappa^*_{m,-m}$ which gives the main contribution to the FS efficiency. The analysis in this case becomes complicated and inaccurate in WKB approximation. More rigorous approach to this case will be developed below in section 3 taking into account that close to the cut-off, where density profile can be supposed linear, accurate solutions of equation (1) are available.

In general case these branching points are situated far from the stationary point, so that their contribution to the integral (17) is a quickly oscillating function of x and q and therefore is negligible. This is easy to show already in the case of profile slightly different from linear when branching point $\varkappa_b$ is not so far from the stationary one to allow us to decompose

$$x_*(\varkappa_b) \approx a + x'_*(\varkappa_b - \varkappa^*)$$

To estimate the contribution of branching point we perform the integration over $\chi = \varkappa - \varkappa_b$ within vicinity of the branching point taking into account that

$$\frac{|\Delta(\varkappa, q)|^2}{|\varkappa|} \approx \frac{\omega}{c(\Lambda_0 - \mathcal{R})}\left[\chi^2 + \left(\frac{\omega\rho^2\varkappa_b}{2c(\Lambda_0 - \mathcal{R})}\right)^2\right]^{-1/2}$$

The phase in (17) takes the form

$$\frac{\mathrm{i}[x - x_*(\varkappa, q)]^2}{2x'_{*\varkappa}} = -\frac{\mathrm{i}\omega k^2(x)\ell_*^6}{c(\Lambda_0 - \mathcal{R})}\left[1 - \left(\frac{\omega\Lambda_*}{2cL_*k(x)}\right)^2\right]q^2 - 2\mathrm{i}k^2\ell_*^2\chi$$

This representation allows us to perform the integration over χ and estimate the integral over q in (17). The ratio between the contributions of the branching and stationary points takes the form

$$\frac{S_b(x)}{S_{FS}(x)} \sim \rho\sqrt{\frac{\omega}{c(\Lambda_0 - \mathcal{R})}}\left|1 - \left(\frac{\omega\Lambda_*}{2cL_*k(x)}\right)^2\right|^{-1/2}$$

The factor on right-hand side of this equation can be estimated as

$$\left[1 - \left(\frac{\omega\Lambda_*}{2cL_*k(x)}\right)^2\right]^{-1/2} \sim \frac{\omega}{ck(x)}\sqrt{\frac{12}{\alpha}}$$

where $\alpha = |L_*^2/n_e(x_c)\cdot \mathrm{d}^2n_e(x)/\mathrm{d}x^2||_{x=x_c}$ characterizes the nonlinearity of the density profile. This leads to the condition (24), when contribution in question can be neglected.

References

[1] Zou X L, Seak T F, Paume M, Chareau J M, Bottereau C and Leclert G 1999 *Proc. 26th EPS Conf. on Contr. Fusion and Plasma Physics (Maastricht)* ECA vol **23J** 1041

[2] Bulanin V V, Lebedev S V, Levin L S and Roytershteyn V S 2000 *Plasma Phys. Rep.* **26** 813

[3] Hirsch M, Holzhauer E, Baldzuhn J, Kurzan B and Scott B 2001 *Plasma Phys. Control. Fusion* **43** 1641

[4] Bulanin V V, Gusakov E Z, Petrov A V and Yefanov M V 2002 *Proc. 29th EPS Conf. on Plasma Physics and Contr. Fusion (Montreux)* ECA vol **26B** P-2.121

[5] Gusakov E Z and Yakovlev B O 2001 *Proc. 28th EPS Conf. on Contr. Fusion and Plasma Physics (Funchal)* ECA vol **25A** 361

[6] Piliya A D and Popov A Yu 2002 *Plasma Phys. Control. Fusion* **44** 467

[7] Gusakov E Z and Tyntarev M A 1997 *Fusion Eng. Design* **34** 501

[8] Gusakov E Z and Yakovlev B O 2002 *Plasma Phys. Control. Fusion* **44** 2525

[9] Gusakov E Z and Popov A Yu 2003 *Proc. 30th EPS Conf. on Contr. Fusion and Plasma Physics (St. Petersburg)* ECA vol **27A** P-2.53

[10] Novik K M and Piliya A D 1993 *Plasma Phys. Control. Fusion* **36** 357

[11] Clairet F, Bottereau C, Chareau J M, Paume M and Sabot R 2001 *Plasma Phys. Control. Fusion* **43** 429

[12] Doyle E J, Staebler G M, Zeng L, Rhodes T L, Burrell K H, Greenfield C M, Groebner R J, McKee G R, Peebles W A, Rettig C L, Rice B W and Stallard B W 2000 *Plasma Phys. Control. Fusion* **42** A237

[13] Lin Y, Nazikian R, Irby J H and Marmar E S 2000 *Plasma Phys. Control. Fusion* **43** L1

[14] Bruskin L G, Mase A, Oyama N and Miura Y 2002 *Plasma Phys. Control. Fusion* **44** 2035

[15] Bulanin V V, Petrov A V and Yefanov M V 2003 *Proc. 30th EPS Conf. on Contr. Fusion and Plasma Physics (St.-Petersburg)* ECA vol **27A** P-2.55

[16] Valeo E J, Kramer G J and Nazikian R 2002 *Plasma Phys. Control. Fusion* **44** L1

[17] Kramer G J, Valeo E J and Nazikian R 2003 *Rev. Sci. Instrum.* **74** 1421

[18] Gusakov E Z and Popov A Yu 2002 *Plasma Phys. Control. Fusion* **44** 2327

[19] Mazzucato E 2001 *Nuclear Fusion* **41** 203

[20] Hirsch M and Holzhauer E 2004 *Plasma Phys. Control. Fusion* **46** 593

[21] Gusakov E Z, Leclert G, Boucher I, Heuraux S, Hacquin S, Colin M, Bulanin V V, Petrov A V, Yakovlev B O, Clairet F and Zou X L 2002 *Plasma Phys. Control. Fusion* **44** 1565